Study of the Interaction of Eu3+ with Microbiologically Induced Calcium Carbonate Precipitates using TRLFS

Johnstone, E. V.; Hofmann, S.; Cherkouk, A.; Schmidt, M.;

Originally published:

October 2016

Environmental Science & Technology 50(2016)22, 12411-12420

DOI: https://doi.org/10.1021/acs.est.6b03434

Study of the Interaction of Eu^{3+} with Microbiologically Induced Calcium Carbonate Precipitates using TRLFS

Journal:	*Environmental Science & Technology*
Manuscript ID	es-2016-034346.R1
Manuscript Type:	Article
Date Submitted by the Author:	04-Oct-2016
Complete List of Authors:	Johnstone, Erik; Helmholtz-Zentrum Dresden-Rossendorf, Institute of Resource Ecology Hofmann, Sascha; Helmholtz-Zentrum Dresden-Rossendorf Cherkouk, Andrea; Helmholtz-Zentrum Dresden-Rossendorf, Institute of Resource Ecology Schmidt, Moritz; Helmholtzzentrum Dresden-Rossendorf, Institute of Resource Ecology

Study of the Interaction of Eu^{3+} with Microbiologically Induced Calcium Carbonate Precipitates using TRLFS

*Erik V. Johnstone, Sascha Hofmann, Andrea Cherkouk, and Moritz Schmidt**

Helmholtz-Zentrum Dresden - Rossendorf, Institute of Resource Ecology, Bautzner Landstrasse 400, 01328 Dresden, Germany.

ABSTRACT

The microbial induced biomineralization of calcium carbonate using the ureolytic bacterium *Sporosarcina pasteurii* in the presence of trivalent europium, a substitute for trivalent actinides, was investigated by time resolved laser-induced fluorescence spectroscopy (TRLFS) and a variety of physicochemical techniques. Results showed that the bacterial-driven hydrolysis of urea provides favorable conditions for $CaCO_3$ precipitation and Eu^{3+} uptake due to subsequent increases in NH_4^+ and pH in the local environment. Precipitate morphologies were characteristic of biogenically formed $CaCO_3$ and consistent with the respective mineral phase compositions. The formation of vaterite with some calcite was observed after one day, calcite with some vaterite after one week, and pure calcite after two weeks. The presence of organic material associated with the mineral was also identified and quantified. TRLFS was used to track the

interaction and speciation of Eu^{3+} as a molecular probe with the mineral as a function of time. Initially, Eu^{3+} is incorporated into the vaterite phase, while during $CaCO_3$ phase transformation Eu^{3+} speciation changes resulting in several species incorporated in the calcite phase either substituting at the Ca^{2+} site or in a previously unidentified, low-symmetry site. Comparison of the biogenic precipitates to an abiotic sample shows mineral origin can affect Eu^{3+} speciation within the mineral.

INTRODUCTION

Biomineralization is the process by which living organisms produce minerals. This phenomenon occurs universally throughout the biological kingdom, yielding a variety of minerals with different compositions, morphologies, and properties. There are three categories of biomineralization: biologically-controlled, biologically-influenced, and biologically induced mineralization.[1-3] For the latter, an array of microorganisms has been reported to induce the precipitation of calcium carbonate minerals, i.e., carbonatogenesis, also referred to as microbial induced calcium carbonate precipitation (MICP).[4] Over 40 different microorganisms have been reported to induce $CaCO_3$ precipitation.[5] Organisms associated with the nitrogen cycle that are able to induce biomineralization, e.g., ammonification of amino acids, nitrate reduction, or urea hydrolysis, have been the most studied.[6-8] Hydrolyzing urea using ureolytic bacteria has proven to be a simple and efficient method for precipitating $CaCO_3$. Mechanistically, when urea (H_2NCONH_2) is metabolized it is converted to NH_3 and dissolved inorganic carbon (Eq. 1), which equilibrate in water increasing the alkalinity (Eq. 2 and 3). The increased pH of the solution, is buffered by the formation of NH_4^+ ($pK_a = 9.24$), but ultimately leads to precipitation

of $CaCO_3$ in the presence of Ca^{2+} (Eq. 4).[6,9-12] Previous studies have shown that varying polymorphs of $CaCO_3$, typically vaterite and calcite, can be produced using this technique.[13]

$$H_2NCONH_2 \rightarrow 2\ NH_3 + CO_2 \quad \text{(Eq. 1)}$$

$$2\ NH_3 + 2\ H_2O \leftrightarrow 2\ NH_4^+ + 2\ OH^- \quad \text{(Eq. 2)}$$

$$2\ CO_2 + 2\ OH^- \leftrightarrow HCO_3^- + OH^- \leftrightarrow CO_3^{2-} + H_2O \quad \text{(Eq. 3)}$$

$$Ca^{2+} + CO_3^{2-} + \leftrightarrow CaCO_3(s) \quad \text{(Eq. 4)}$$

MICP has gained much interest as a geobiological tool for addressing a variety of environmental, agricultural, and architectural problems.[4,14-16] For example, these include soil and water remediation, formation of underground barriers, lake and reservoir sealing, concrete and limestone restoration, and CO_2 sequestration.[4,15] From an environmental remediation focus, the use of MICP has been suggested for the sequestration, retardation, or even complete removal of toxic and harmful contaminants. These contaminants include toxic metals[17,18] and radioactive elements, e.g., U and ^{90}Sr.[13] Particularly concerning these radioelements, most studies have been aimed at the cleanup and removal of ^{90}Sr from contaminated nuclear legacy sites, which include the proposed use of bioengineering techniques such as pulse-flow injection.[19-21] Results have shown effective Sr^{2+} uptake and immobilization into biogenic $CaCO_3$. Using XAS Fujita et al. observed the formation of a solid solution with Sr^{2+} substitution at the Ca^{2+} site within calcite lattice.[20]

The long-lived, highly radiotoxic transuranic elements, i.e., neptunium, plutonium, americium, and curium, as well as some lanthanide fission products, e.g. ^{155}Eu,[22] are a major environmental concern. They are man-made elements or nuclides, resulting from nuclear processes that have

been or will be introduced into the biosphere during geologic disposal, nuclear accidents, and in nuclear weapons fallout.[23,24,25] The progressively widespread use of lanthanides in technological devices and as medical imaging agents also increases possibilities of contamination of the environment.[26] Additionally, some trivalent lanthanides/actinides exhibit similar size and coordination geometry to Ca^{2+}, which allows these elements to follow Ca^{2+} in biological systems, e.g. by incorporation into bones [Holliday et al.].[27] When considering their radio- and chemotoxicities, this behavior can be particularly harmful for biota, thus schemes for their reuse and/or disposal should be developed.

Previous studies have determined that trivalent americium[28] and curium[29] as well as their homologous lanthanides[30-32] are strongly partitioned into phases of $CaCO_3$. The interactions of these elements with $CaCO_3$ are often dominated by surface sorption or incorporation, where incorporation can occur either in the bulk structure or at the Ca^{2+} position in the crystal lattice via substitution.[32-34] Although an appreciable amount of natural calcite is of biogenic origin and can host a substantial amount of Eu^{3+},[35] never have the interactions of trivalent rare earth or actinide elements with biogenic $CaCO_3$ been systematically studied. Comparatively, the bio(apatite) system has been investigated, and it was revealed that these elements interact with biogenic apatite considerably different than with the inorganically derived mineral. Results showed that Eu^{3+} was found incorporated in the grain boundaries of the lattice and not at either of the Ca^{2+} sites within the mineral as was previously reported. This difference in structural localization can have significant implications when considering actinide sequestration in human bone.[36,37] With $CaCO_3$ ubiquitously occurring throughout the bio- and geosphere, found in shells and skeletal components and in the mineralogy of many nuclear repositories, this raises the question if similar

effects may be found for biogenic $CaCO_3$, i.e., if there are differences in how trivalent actinides and lanthanides interact with abiotic and biotic $CaCO_3$.

Time resolved laser-induced fluorescence (TRLFS) is an important and versatile tool for studying mineral interactions with luminescent trivalent actinides and lanthanides, i.e., Eu, Am, and Cm.[23,28,29,38,39] This characterization tool allows the site-selective excitation of a fluorescent probe in low concentrations (~ 10^{-7} M Eu^{3+}) to determine discrete species present with a mineral. From this, detailed information of probe symmetry from characteristic emission band splittings and extent of hydration from measured fluorescent decay lifetimes can be determined for the differentiation of species that are either surface sorbed or incorporated in the mineral.[40] In turn, this may help to evaluate the stability of the formed solid solution more accurately as well as the geochemical properties of trivalent actinides and lanthanides associated with $CaCO_3$.

The aim of this study was to gain a better understanding of the process of biomineralization of $CaCO_3$ and how trivalent actinide or lanthanide elements could potentially interact with it. Calcium carbonate was precipitated via ureolysis using *Sporosarcina pasteurii*, an archetypal ureolytic bacterium, in the presence of Eu^{3+} and studied using a variety of analytical techniques. TRLFS was used to investigate the behavior of Eu^{3+} with the resulting mineral. The effect of biogenic components incorporated into the mineral on Eu^{3+} speciation was compared to an abiotic sample synthesized under similar conditions.

EXPERIMENTAL

Culturing and Inoculation. The strain *Sporosarcina pasteurii* (DSM33, ATC11859) was cultured in CASO medium (Merck 105458) (15 g/L peptone from casein, 5 g/L peptone from soymeal, 5 g/L NaCl, pH = 7.3) amended with 20 g/L urea at 30 °C on a rotary shaker (80 rpm)

overnight. For the inoculation, cultures were transferred into fresh media and grown at 30 °C for approximately 15 hours. The bacteria were harvested from a 50 mL aliquot using a rotary centrifuge (8,820 rcf) for 15 minutes. The supernatant was removed and the resulting cell pellet was resuspended and washed two times with 50 mL of medium containing 20 g/L urea, 10 g/L NH_4Cl, and 2.12 g/L Na_2CO_3 in MilliQ filtered water and pH adjusted to 5.6. The cell pellet was then diluted in the same medium until an optical density reading at 600 nm (OD_{600}) using a spectrophotometer (Cary 50 Bio) with a 1 cm path length of 0.40 ± 0.02.

Mineralizing Medium. The $CaCO_3$ mineralizing medium used was similar to that reported by Stocks-Fischer (1999).[6] This was prepared by mixing of two solutions: a first solution of 3.0 g bacterial nutrient broth in 800 mL of MilliQ filtered water at pH adjusted to 5.6 with the dropwise addition of concentrated HCl(aq), which was then autoclaved. A second solution was prepared by dissolving 20 g urea, 10 g NH_4Cl, and 2.12 g Na_2CO_3 in 180 mL of MilliQ filtered water and pH adjusted to 5.6. To this solution 3.7 g $CaCl_2{\cdot}2H_2O$ and a 100 µL aliquot of a $1.0x10^{-3}$M solution of $EuCl_3{\cdot}6H_2O$ were added, the pH was readjusted again to 5.6, and the final volume adjusted to 200 mL. The second solution was filter sterilized through a 0.2 µm filter and combined with the first for a final stock solution containing 3.g/L nutrient broth, 20 g/L urea, 10 g/L NH_4Cl, and 2.12 g/L Na_2CO_3, 3.7 g/L $CaCl_2{\cdot}2H_2O$, and $1.0x10^{-7}$ M $EuCl_3{\cdot}6H_2O$.

$CaCO_3$ Precipitation Experiments with Europium. Experiments were performed using sterile handling techniques under aerobic conditions. The mineralizing medium stock (150 mL) was transferred into two different 250 mL Erlenmeyer flasks each, and 1 mL of the previously described inoculum containing *S. pasteurii* was added to one of the flasks for a calculated starting OD_{600} = 0.003 and a 1 mL aliquot of medium containing no bacteria added to the control. The bacterial and abiotic control flasks were kept at 30 ºC on a rotary shaker (80 rpm).

Samples (1 mL) were collected from both flasks at varying times throughout the duration of the experiment into 1.5 mL centrifuge tubes, centrifuged at 16,100 rcf at 25 ºC for 5 minutes, and the supernatants were removed. The pH was determined immediately, while samples for inductively coupled plasma mass spectrometry (ICP-MS) measurements and determination of [NH_4^+] were stored at 4 ºC until measured. In addition, mineral formed in the flasks containing bacteria was sampled with a pipette during the duration of the experiment at different times and monitored with light microscopy. Experiments were run for durations of either one day, one week, or two weeks. All experiments were performed in triplicate.

At the end of each experiment, the supernatant containing the biomass was removed from the precipitate by decantation. Subsequently, the reaction flask containing was scraped with a sterilized glass rod to remove any adhered precipitate and the precipitate was transferred into a sterile centrifuge tube. The precipitate was washed twice with MilliQ water and twice with acetone, lightly capped, and air-dried. Precipitate from the triplicate samples for one day, one week, and two weeks were then characterized using a variety of physicochemical instrumental methods unless stated otherwise.

Because it was of interest to distinguish between the impact of biogenic components and that of the growth medium on the interaction of Eu^{3+} with the mineral, an abiotic precipitate was synthesized for comparison with the biogenic $CaCO_3$. In the absence of bacteria, mineralization was induced by dropwise titration of the Eu^{3+}-containing mineralizing medium (150 mL) with an NaOH solution until pH ~ 9.2. The resulting sample was incubated for 10 days at 30 ºC on a rotary shaker (80 rpm) and the precipitate was harvested using the same techniques as above. The resulting sample, which will be referred to as the abiotic precipitate, was analyzed by TRLFS

Characterization Methods. *Time Resolved Laser-Induced Fluorescence (TRLFS)*. TRLFS can be used for determining the local coordination environment of the Eu^{3+} ion. The non-degenerative (J = 0) excitation of the ground state $^7F_0$ to the excited state $^5D_0$ yields a single peak for each respective species. Excitation spectra can be produced by probing the sample with varying excitation wavelengths and measuring the integrated fluorescence yield. For the Eu^{3+} $^7F_0 \rightarrow {}^5D_0$ transition an appropriate excitation wavelength window ranges from 577 nm to 582 nm. Direct excitation of each species yields a characteristic emission spectrum and fluorescence lifetime. Splitting patterns of the ($^5D_0 \rightarrow {}^7F_1$) and ($^5D_0 \rightarrow {}^7F_2$) bands can be used to determine the local site symmetry of the Eu^{3+} ion which can be compared to the crystallography of the host mineral.[40] Higher splitting patterns of these transitions are indicative of lower site symmetry with a maximum splitting equal to (2J + 1).[40]

Fluorescence lifetimes can be empirically correlated to the degree of hydration where shorter lifetimes, i.e., < 1700 μsec, are a result of non-radiative energy transfer to OH-oscillator vibrations, and longer lifetimes, i.e., ≥ 1700 μsec, indicate no bound water associated with the Eu^{3+} ion. Employing Horrocks and Sudnick's equation (Eq. 5) the decay constant k ($1/\tau$) correlates to the amount of quenching water molecules where τ is in milliseconds.[41]

$$n(H_2O) = 1.07k - 0.62 \qquad \text{(Eq. 5)}$$

The measured lifetime and degree of hydration provide insight into the speciation of Eu^{3+} either in solution or in the presence of a solid interface. For example, the Eu^{3+} aquo-ion yields a low fluorescence lifetime, i.e., τ = 110 μsec, that equates to 9 H_2O in its inner coordination sphere, whereas when it is fully incorporated into the crystal lattice of a mineral, such as calcite, longer lifetimes are obtained, i.e., τ > 3600 μsec, equivalent to 0 H_2O present.[32]

TRLFS was performed using a pulsed (10 Hz) Nd:YAG (Spectra Physics, 532 nm) pumped dye laser (Radiant Dyes). The laser dye Pyrrhomethene 580 was used for direct excitation of Eu^{3+} in the range from 575–582 nm. The laser wavelength and power were monitored using a wavemeter (High Finesse WS-5) (>10^{-5} nm accuracy) and power meter (Newport 1918-R), respectively. Fluorescence measurements were detected by an optical multichannel analyzer that consists of a monochromator with 300/600/1200 lines/mm gratings (Acton SpectraPro 300i) and an intensified CCD (Princeton Instruments). Maximum resolution at 300 and 1200 lines/mm was measured to be 0.9 and 0.2 nm, respectively. The detection system was calibrated with a neon lamp (Pen Ray 6032). The samples were cooled to ~ 10 K by a helium refrigerated cryostat (CTI-cryogenics) to improve resolution. To avoid camera exposure to the direct laser beam, the minimum gate delay between laser pulse and camera gating was set to 1.0 μs. The gate width of the camera was fixed at 10 ms to ensure the collection of the entire fluorescence signal. Fluorescence lifetime measurements were made with a delay time step between 50 and 150 μs and a total of 100 steps were taken for each lifetime measurement.

Microscopy and Mineral Composition Analysis. Precipitates for light microscopy imaging were directly sampled from solution, separated from the supernatant, and washed with sterile MilliQ water. The samples were resuspended in water (~4 μL) and pipetted onto glass slide, covered with a glass coverslip, and imaged using an Olympus BX61 light microscope. Samples for scanning electron microscopy (SEM)/energy dispersive X-ray spectroscopy (EDX) were prepared by transferring the precipitate in MilliQ water onto a silicon wafer and dried in a desiccator at ambient temperature. The samples were imaged with a Zeiss EVO 50 SEM equipped with a Bruker AXS QUANTAX 200 EDX. Mineral phase composition was determined with a Bruker D8 powder X-ray diffractometer or a RIGAKU MiniFlex 600. Precipitates were

pulverized in an agate mortar and the resulting powders were evenly dispersed on a low-background silicon wafer and measured from 18º to 50º 2θ with a step size of 0.02º 2θ. Thermal gravimetric analyses (TGA) were conducted on one representative of the triplicate samples from the one day, one week, and two week experiments. Samples were measured in a Mettler Toledo TGA with a TG 50 furnace unit. A sample of 20 to 40 mg were heated in a ceramic crucible under a nitrogen atmosphere (100 ml/h) over the range of 35 to 850 ºC at a rate of 10 ºC/sec. Multi-point N_2-BET surface area of the precipitate after two weeks (Brunauer-Emmett-Teller theory) was determined using a surface area and pore size analyzer (mod. Coulter SA 3100, Beckman Coulter, Fullerton, USA). Weighed quantities of the resulting precipitates were dissolved in 30% HNO_3, and the Eu^{3+} concentration for each sample was determined using ICP-MS (NexION 350 X, PerkinElmer).

Solution Chemistry Analysis. The pH was measured using a Mettler Toledo Inlab® electrode and calibrated with pH = 4, 6, and 9 standard solutions (WTW, Weilheim, Germany). Ammonium-ammonia concentration was determined using an ammonium ion selective electrode with Nernstian response and measured against a calibration curve (WTW, Weilheim, Germany). Supernatants collected were acidified with HNO_3 (1 %), and Eu^{3+} and Ca^{2+} concentrations were determined using an ICP-MS. All measurements were made in triplicates.

RESULTS

Biomineralization Precipitation Experiments. In mineralizing medium containing Eu^{3+} and urea, *S. pasteurii* demonstrated ureolytic behavior consistent with the liteature.[6,13,20] As shown in Figure 1A, pH and NH_4^+ concentrations increased rapidly within the first 6 hours and reached maximum values after 48 hours of 9.2 and 1.0 mol/L, respectively. The decrease of NH_4^+

concentrations over time was caused by the release of $NH_3(g)$ in equilibrium with NH_4^+ at this pH. An initial increase in pH of the abiotic control was observed reaching pH = 7.2 after 24 hours, although no significant amount of paralleled NH_4^+ production was detected. Notably, induced mineral precipitation was consistently observed in the bacterial samples under these conditions after 3 to 4 hours of reaction time between the pH range of 7.8 and 8.0. For the abiotic control samples, no mineral precipitation was observed throughout the duration of the experiment. This trend was also evident when tracking soluble Ca^{2+} and Eu^{3+} concentrations.

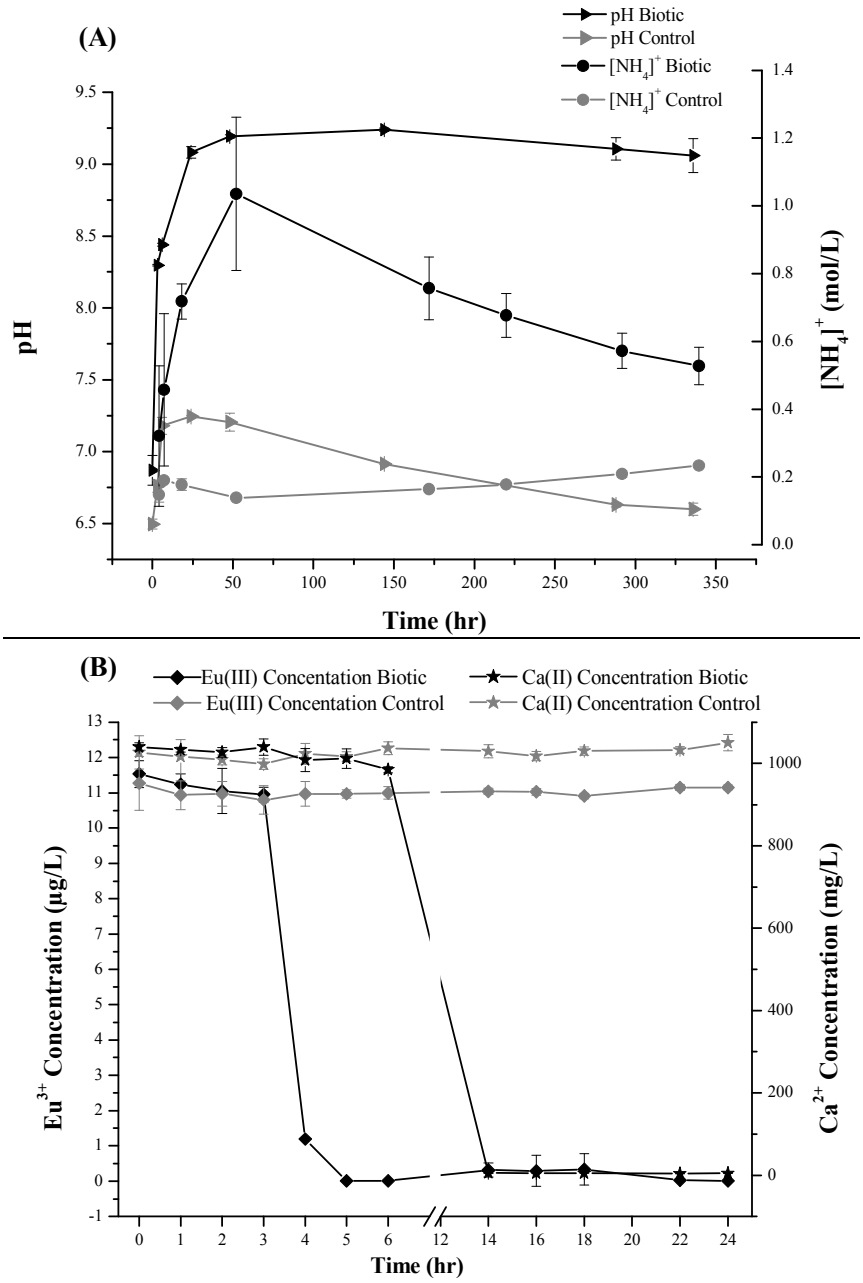

225

226

227 **Figure 1.** (A) Measured pH and total NH_4^+ in solution in biotic (black triangles and black circles,

228 respectively) and control (grey triangles and grey circles, respectively) cultures as a function of

229 time. (B) Eu^{3+} and Ca^{2+} concentrations measured in the solution in biotic (black diamonds and

230 black stars, respectively) and control (grey diamonds and grey stars, respectively) cultures as a

function of time. Points represent the average of triplicate measurements and error bars represent the standard deviation.

The change in soluble Eu^{3+} and Ca^{2+} concentrations was tracked and measured by ICP-MS as shown in Figure 1B. In the cultures containing *S. pasteurii*, no drastic consumption of either Ca^{2+} or Eu^{3+} was observed in the first 3 hours of the experiment. After this "induction phase," europium concentration in solution decreased rapidly. To note, the earlier onset of the decrease in Eu^{3+} does indicate precipitation of a Eu^{3+} solid phase. A significant decrease in Ca^{2+} concentration did not occur until later between the 6^{th} and 14^{th} hours of the experiment. Concentrations of Eu^{3+} and Ca^{2+} reached 0.01 μg/L and 4.35 mg/L and were stabilized after 5 and 14 hours, respectively, and no leaching of Eu^{3+} was observed following precipitation. Conversely, in the abiotic control the concentrations of both elements remained constant and the formation of any precipitates was not observed.

Mineral Characterization. *Particle Formation and Morphology*. Light microscopy was used to monitor the precipitation of biogenic $CaCO_3$ examining morphology, size, and distribution of the mineral. Figure S1 (Supplementary information) displays images of the formation and crystallization of biomineralized $CaCO_3$ at various times over a two-week period. Initial samples collected after three hours show small, undefined precipitates surrounding and closely associated with the bacteria. After six hours, precipitates were observed with discrete shapes ranging in size from 10 to 40 μm. After one day, precipitates ranging up to 50 μm were present exhibiting framboidal morphology. After one and two weeks, precipitates were found ≤ 50 μm in diameter with defined faces and edges. The average surface area per mass of the bulk precipitate collected after two weeks was measured by BET to be 0.42 ± 0.02 m^2/g.

253 SEM was employed to better understand the formation and development of the precipitate
254 morphology from particle to aggregate level. In Figure 2A, the image of precipitate harvested
255 after one day shows small particles with distinct spherical shapes consistent with the vaterite
256 morphology. Other morphologies, e.g., anhedral irregular, hemi-spherulite, and discoid, that have
257 been reported[43] for biogenic carbonates were also found here. On the surfaces of some of the
258 precipitates, pitting resembling bacteria morphology was observed. After one and two weeks
259 (Figure 2B-D), precipitate morphologies were more euhedral/subhedral and resembled those
260 reported for calcite with characteristic rhombohedral faces. In addition, particle size distribution
261 of these precipitates ranged from approximately 2 to 150 μm. EDX analyses of the precipitates
262 (Figure S2) yielded C, O, and Ca as expected for $CaCO_3$. Comparatively small amounts of P and
263 Mg were also identified that most likely originate from the cellular composition of the bacteria.
264 The sensitivity of the EDX analyses was not high enough to detect Eu^{3+} at the concentration
265 used. A weighed quantity of each of the precipitates was dissolved and the Eu^{3+} concentration
266 was measured by ICP-MS. The concentrations after one day, one week, and two weeks were
267 470 ± 47 μg g^{-1}, 546 ± 55 μg g^{-1}, and 531 ± 53 μg g^{-1} Eu^{3+}, respectively.

268

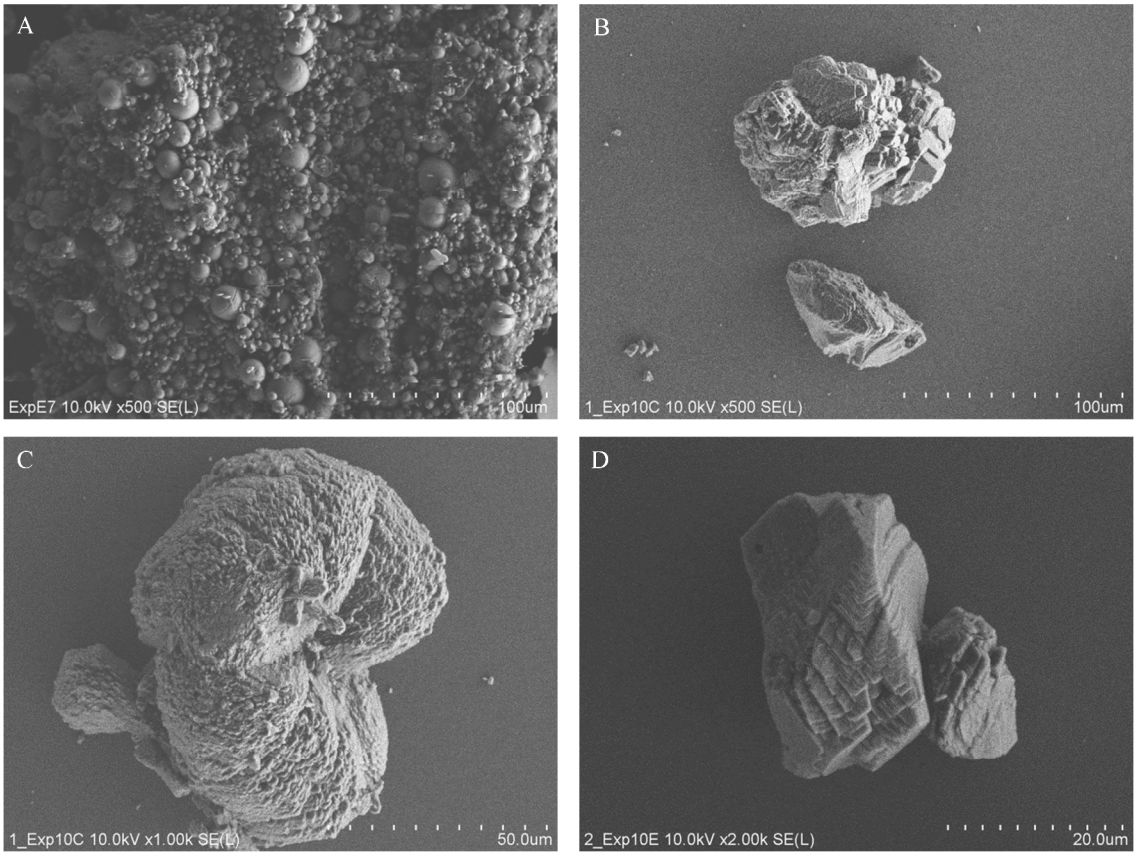

Figure 2. SEM images of biogenic $CaCO_3$ at various times: A) 24 hours, B and C) 1 week, and D) 2 weeks. Scale bars provided at the lower right hand of each image.

Particle Composition Analysis. The mineralogical compositions as a function of time were characterized by powder XRD. As shown in Figure 3, the relative abundance of the identified phases, i.e., vaterite and calcite, of the biogenic $CaCO_3$ changed over time. Vaterite was the predominant phase found after 24 hours, and although the (104) peak of calcite was also observed, it was very weak indicating calcite was a minor phase at this time. After one week the sample also exhibited a mixture of vaterite and calcite, but with calcite as the major constituent. Using the XRD method reported by Dickinson and McGrath[44] for estimating relative phase compositions, the samples were found with 9 ± 5 wt% calcite and 91 ± 5 wt % vaterite after one day and 85 ± 5 wt% calcite and 15 ± 5 wt% vaterite after one week. The complete transformation

to calcite was observed after 2 weeks. The phases present at the respective times were consistent with morphologies observed by imaging techniques (Figure 2). For the abiotic precipitate after 10 days, a relative phase composition of 14 ± 5 wt% calcite and 86 ± 5 wt% vaterite was determined.

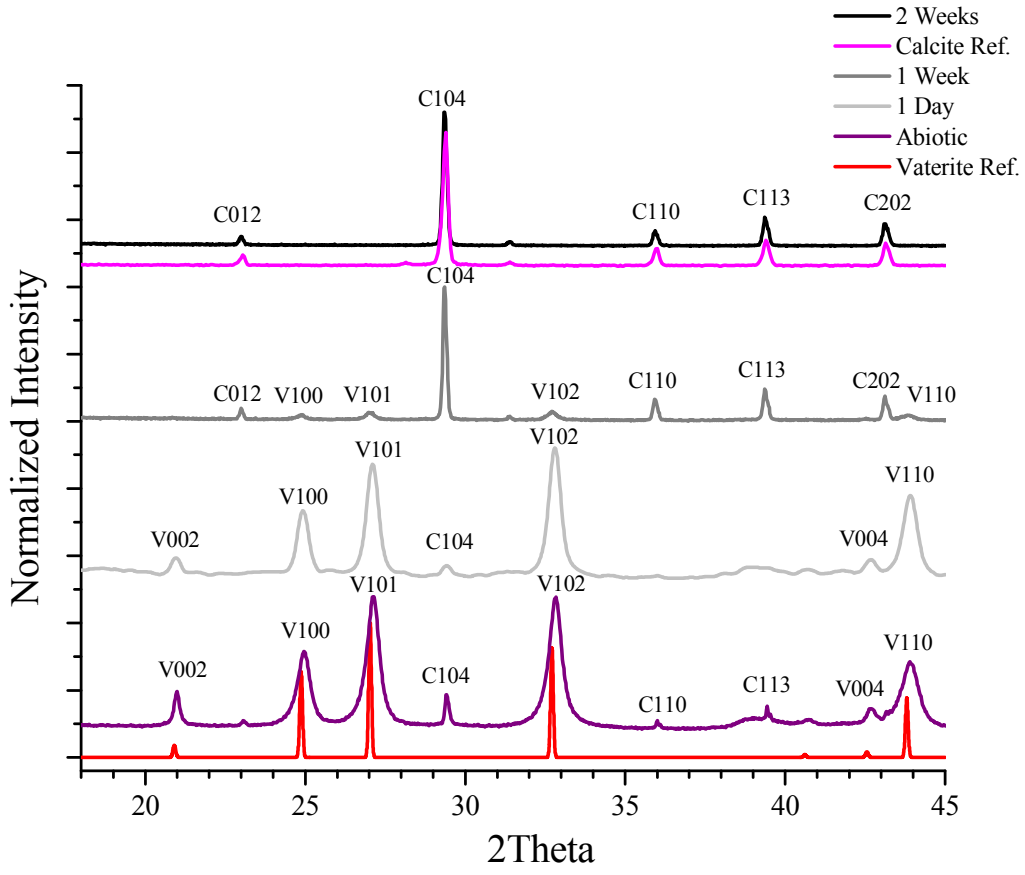

Figure 3. A comparison of XRD powder patterns of biomineralized $CaCO_3$ from *S. pasteurii* after one day, one week, and two weeks, and abiotic $CaCO_3$ after 10 days. Peaks are labeled with the calcite (C) or vaterite (V) and the respective Miller indices [HKL].

Thermal gravimetric analysis was used to determine the amount of remaining organic material in the precipitate after recovery and washing. Figure S4 displays the thermal behavior of samples precipitated at different times versus a calcite standard. In comparison with an abiotic calcite

standard, which showed no significant loss of mass before ~ 750 ºC, a two-step change in mass in this range was observed for the biogenic $CaCO_3$ samples. This can be attributed to the loss of water associated with the mineral up to 200 ºC, and the loss of organic material from 200 to 650 ºC.[45] From this, it was determined that the sample after one day contained about 6 wt% organic matter, whereas the one and two week samples contained about 2 wt%. Final decomposition temperatures of $CaCO_3$ to CaO and CO_2 were approximately 795, 818, and 837 ºC for the $CaCO_3$ after one day, two weeks, and one week, respectively. These decomposition temperatures were notably lower than the calcite standard measured at 842 ºC. This has been attributed to the presence of crystal defects due to crystal grain growth speed and the inclusion of trace elements, e.g., Mg^{2+}, into the lattice during crystallization, which can distort and lower the stability of the crystal lattice.[46,47]

Europium TRLFS: Analysis and Speciation. *Precipitate After One Day.* The excitation spectrum of the Eu^{3+} doped biogenic $CaCO_3$ after one day is shown in Figure 4. In the spectrum, only a single absorption maximum was observed at 579.1 nm corresponding to one species, which will be designated as Species I. The luminescence lifetime of Species I (Table 1, Figure S4) was measured after selective excitation at 579.1 nm and characterized by monoexponential behavior with a value of $\tau = 4550 \pm 580$ μsec. This lifetime value is consistent with 0 coordinating H_2O molecules and incorporation of Eu^{3+} in the mineral phase. For the emission spectrum (Figure 5), a two-fold splitting of the $^5D_0 \rightarrow {}^7F_1$ and a three-fold splitting of the $^5D_0 \rightarrow {}^7F_2$ transitions were observed. Comparatively, the emission spectrum and lifetime are consistent with the Eu^{3+} incorporated vaterite species substituted at the Ca^{2+} site.[32]

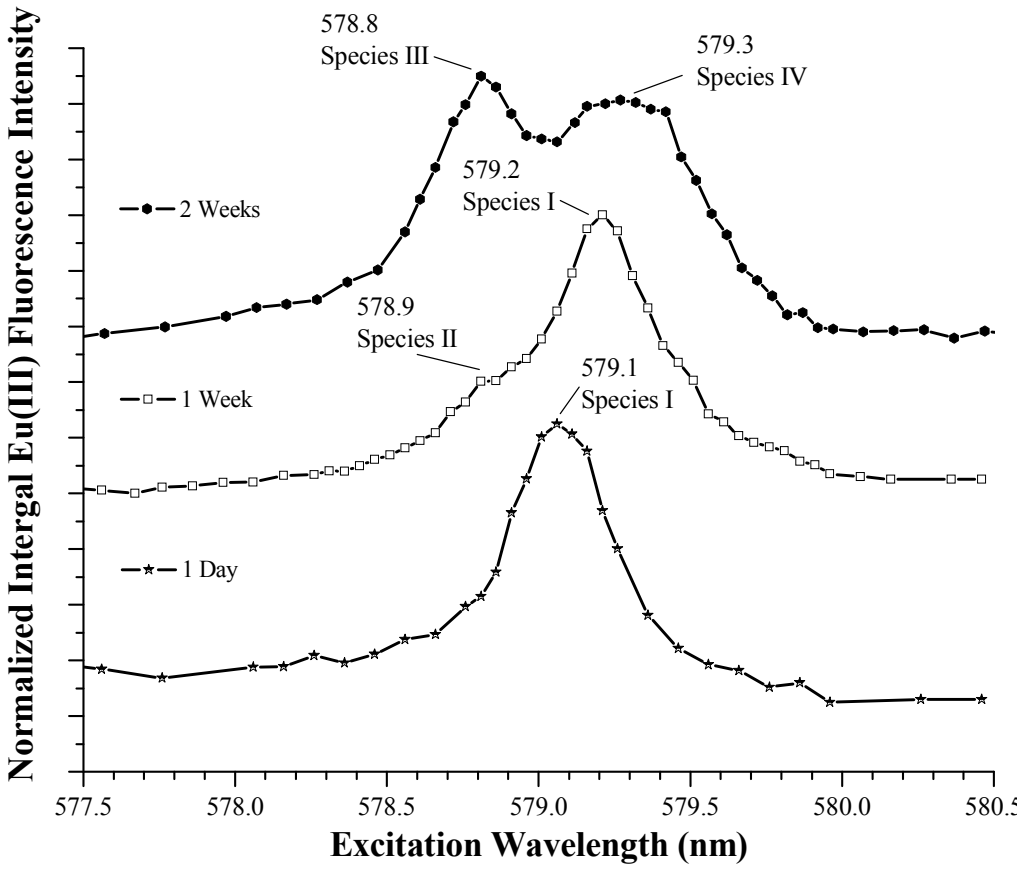

Figure 4. The $^7F_0 \rightarrow {}^5D_0$ excitation spectra of the Eu^{3+} containing biogenic $CaCO_3$ produced by *S. pasteurii*.

Precipitate After One Week. After one week, two different excitation species were observed (Figure 4). The speciation here is still dominated by Species I, which exhibited an identical emission spectrum and lifetime compared to the same species after one day. Its excitation maximum had shifted, however, to 579.2 nm. This is explained by spectral overlap with a second species as a much less intense shoulder at 578.9 nm.

The shoulder located at 578.9 nm is unique and must be indicative of the presence of a second species, which will be referred to as Species II. Excitation at 578.9 nm yielded a characteristic

biexponential fluorescence decay behavior, a property when multiple species are simultaneously excited. A biexponential fit was used and a short and a long component could be derived as $\tau_1 = 1100 \pm 140$ μsec and $\tau_2 = 4070 \pm 530$ μsec, respectively. The long component is identical within the errors of measurement for the lifetime of Species I, hence the short lifetime must be characteristic for Species II. Using Horrock's equation, the value of the short lifetime is equivalent to ~0.5 H_2O molecules coordinated to the Eu^{3+}. This slight hydration suggests that Species II occurs within the solution-solid interface, although primarily still bound within the mineral. Species II can be compared with the transition species identified by Schmidt et. al shown in Table 1.[32] The emission spectrum (Figure 5) of Species II is characterized by both a $^7F_1$ and a $^7F_2$ band with a four-fold splitting. In particular, the magnitude of splitting of the $^7F_1$ band exceeds the maximum number of possible $(2J + 1)$ sublevels, which again indicates that multiple species have been simultaneously excited at this wavelength. These results are also consistent with the multiexponential lifetime decay pattern.

337 **Table 1.** Fluorescence emission lifetimes of Eu^{3+} species found in biogenic and abiotic
338 precipitates synthesized in mineralization medium (italics, this study) vs. abiotic vaterite[32] and
339 calcite[49].

Species	$\lambda_{excit.}$ (nm)	Lifetime (μsec)	$n(H_2O)$
Species I, One day	*579.1*	*4550 ± 580*	*0*
Species I, One week	*579.2*	*4330 ± 560*	*0*
Species II	*578.9*	*1100 ± 140*	*0.5*
Species III	*578.8*	*2780 ± 360*	*0*
Species IV	*579.3*	*3380 ± 300*	*0*
Abiotic Precipitate	*579.5*	*2040 ± 260*	*0*
*Vaterite Incorporated	579.3	4069 ± 244	0 [32]
*Transition Species	579.1	1106 ± 133	0.5 [32]
**Calcite Sorption A	578.1	412 ± 49	1-2 [49]
**Calcite Incorporated B	578.4	4368 ± 524	0 [49]
**Calcite Incorporated C	579.6	4352 ± 261	0 [49]

340 * Vaterite samples were precipitated by bubbling CO_2(g) through a $CaCl_2$ (1 M) and NH_4OH (2
341 M) solution containing 20 ppm Eu^{3+} and suspended in a $CaCO_3$ saturated solution for vaterite to
342 calcite transformation.
343 ** Calcite samples were produced in a mixed-flow reactor with a calcite seed crystal and input
344 solutions of $Ca(ClO_4)_2$ (2 mM), $NaHCO_3$ (1.8 mM)/Na_2CO_3 (0.15 mM), and Eu^{+3} (~ 10^{-7} M).
345

346 *Precipitate After Two Weeks*. Two defined excitation peaks were identified in the sample after
347 two weeks shown in Figure 4: a peak at 578.8 nm and a broad peak centered at 579.3 nm. The
348 species at 578.8 nm exhibited a long lifetime of 2780 ± 360 μs with a monoexponential decay
349 profile. This value corresponds to a complete loss of hydration. The correlating emission
350 spectrum shown in Figure 5 is characterized by a six-fold split $^7F_1$ band and a $^7F_2$ band with a
351 minimum of five-fold splitting. Again, this magnitude of splitting is consistent with the
352 excitation of multiple species. Notably, this species at 578.8 nm is unique from the other species
353 identified here and those in prior TRLFS studies of the Eu^{3+}-$CaCO_3$ system, hence it will be

354 referred to as Species III. It is speculated that Species III represents Eu^{3+} incorporated within a
355 low symmetry site in the calcite, although its precise local environment cannot be specified.

356 The lifetime of the species at 579.3 nm was measured with a value of 3380 ± 300 μsec, which is
357 consistent with a complete loss of hydration and Eu^{3+} incorporation. A two-fold splitting and
358 three-fold splitting of the $^7F_1$ and $^7F_2$ band, respectively, are observed in the emission spectrum
359 (Figure 5). This splitting pattern is characteristic of Eu^{3+} incorporated into the trigonal C_{3i} Ca^{2+}
360 site within the calcite lattice.[32-34,49] The lifetime value and emission spectrum of this species is
361 significantly different to the other species in this study, and therefore will be referred to as
362 Species IV. However, it is noted that Species IV is the same species as Species C identified in
363 previous TRLFS investigations of Eu^{3+} with calcite (Table 1 and Figure 5), which has been
364 described as Eu^{3+} substituting Ca^{2+} on a nearly undistorted lattice site.[32-34,49] Because of the
365 broadness of the peak, excitations at 579.2 nm and 579.5 nm were also performed to ensure only
366 one species was present. The results from excitation at these wavelengths were identical with
367 those at 579.3 nm.

368 It is noteworthy that no calcite surface sorption species were observed in the precipitates after
369 one and two weeks. The second calcite incorporation species, Species B, which has been
370 reported in the literature, was also not identified (Table 1).[32,33,49]

371 *Abiotic Precipitate After 10 Days.* As recent investigations have shown, the growth medium may
372 have a significant impact on the calcite surface,[48] and the uptake of trivalent cations by the
373 mineral.[39] To confirm the findings made in this study were due to microbial activity and not the
374 growth medium, mineral was precipitated from the growth medium in the absence *S. pasteurii*
375 and analyzed by TRLFS. The excitation spectrum (Figure S5) of the abiotic precipitate after 10

376 days was measured and a single, broad peak centered at approximately 579.5 nm was identified.
377 Excitation at 579.5 nm yielded a luminescent lifetime of 2040 ± 260 µsec (Table 1), which
378 equates to 0 H_2O molecules in the coordinating sphere the Eu^{3+} species and incorporation into
379 the mineral. The emission spectrum shown in Figure S6 is characterized by a three-fold split $^7F_1$
380 band and a $^7F_2$ band with a minimum of four-fold splitting. From the lifetime and emission data,
381 this Eu^{3+} species can be interpreted as being incorporated into the bulk of the mineral, although
382 in a low-symmetry site. Notably, this species is unique in comparison to Species III and the other
383 species identified in this study as well as those identified in previous TRLFS studies. Therefore,
384 it is difficult to speculate if Eu^{3+} incorporation occurs in the vaterite or calcite phase, however,
385 these results demonstrate the bacteria can affect Eu^{3+} speciation differently than just the medium.

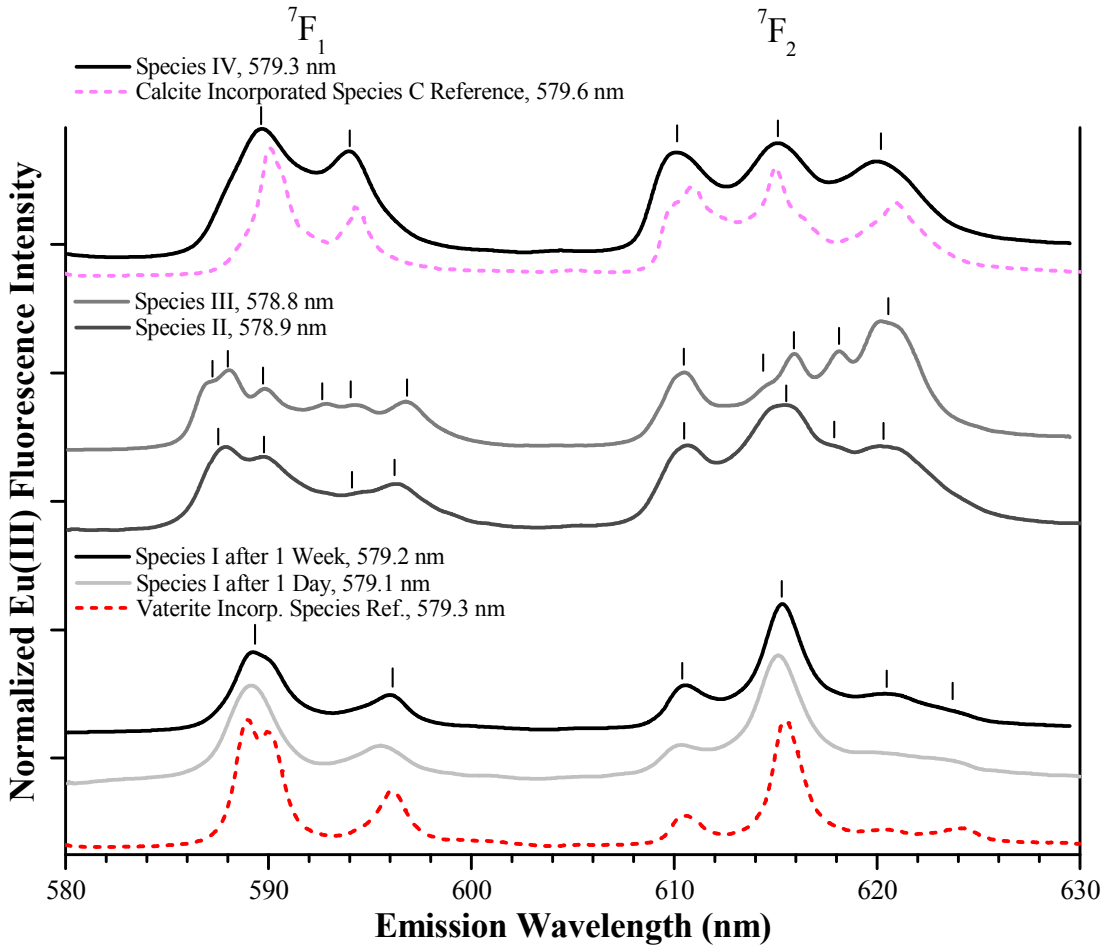

386

Figure 5. The $^5D_0 \rightarrow {}^7F_{1,2}$ emission spectra collected from the site-specific excitation of Eu^{3+} in biomineralized $CaCO_3$. Black dash marks indicate splitting peaks.

DISCUSSION

In the presence of Eu^{3+}, *S. pasteurii* demonstrated capable ureolytic activity under the experimental conditions consistent with the literature.[6,13,20] This yielded a significant increase in alkalinity of the growth medium, which could be measured by both pH and $[NH_4^+]$. The NH_4^+ resulting from ureolysis buffered the medium at pH = 9.2, a pH substantially more alkaline than necessary for $CaCO_3$ precipitation, i.e., pH ~ 8.3.[6] The uptake of free Ca^{2+} and Eu^{3+} ions coincided with $CaCO_3$ precipitation and both were essentially depleted from solution after 14 hours. TRLFS results showed no surface sorbed Eu^{3+} species present with either the vaterite or calcite after one day. Surface sorbed species have been reported in batch and mixed-flow studies with inorganic $CaCO_3$ where surface interactions of Eu^{3+} with the mineral occur before incorporation.[32,34,49] This suggests that the Eu^{3+} was either co-precipitated with the $CaCO_3$ or completely incorporated into the vaterite after one day. After the onset of precipitation, the bacterium and small aggregates of the mineral were in close association, providing evidence for bacterial involvement during the mineralization process.[6] The resulting precipitates were characteristic of biogenic vaterite and calcite and contained between 2 to 6 weight percent of organic material as well as trace element inclusions such as Mg and P.

At least up to one week, Eu^{3+} was found preferentially incorporated in the vaterite phase (i.e., Species I), or to a lesser degree as a transition species (i.e., Species II), at the mineral-solution interface. Notably, no Eu^{3+} was found associated with the calcite phase, even with it being the

409 predominate phase present in the mineral composition after one week. These trends suggest that
410 the incorporation of Eu^{3+} in biogenic vaterite undergoes slower phase transformation to calcite in
411 comparison to vaterite without Eu^{3+}. The presence of a hydrated transition species confirms that
412 the phase transformation from vaterite to calcite is a solution-mediated process and is consistent
413 with the literature.[32]

414 In this study, no sorption species were identified within the timeframe of the experiment. The
415 formation of surface sorbed species with calcite has been identified in mix-flowed reactor and
416 batch studies resulting from mineral dissolution-reprecipitation under steady-state and mineral
417 growth conditions.[32,34,49] This is likely attributed to the lower mineral solubility,[8] which would
418 also prevent significant leaching of either Ca^{2+} or Eu^{3+} after mineral precipitation, observed
419 under these conditions. Previous studies have shown that MICP minerals can behave notably
420 different than their abiotic counterparts due to organic and trace element inclusions and high
421 variability in mineral morphologies and surface topologies originating from their biogenic
422 formation.[50,51]

423 A new Eu^{3+} species, Species III, was identified in the calcite phase incorporated in a low-
424 symmetry environment. This species was not identified in the abiotic sample, nor has it been
425 reported in previous Eu^{3+} TRLFS studies with calcite. The literature has shown that the origin of
426 the mineral can significantly impact the possible interactions of doping elements within the
427 mineral, such as for the bioapatite system.[36,37] Considering the mineral composition, it is
428 speculated that Species III could reside in the organic matrix, organic-mineral interface, and/or
429 another low-symmetry coordination environment in the calcite. However, the presence of
430 Species IV, which is incorporated at the Ca^{2+} site in the lattice, also demonstrates that the
431 substitution of Eu^{3+} for Ca^{2+} is still thermodynamically favored under these conditions.[32-34,49]

Ultimately, both Species III and Species IV are incorporated and essentially sequestered within the calcite precipitate. When considering contaminate retardation or removal in natural or engineered environmental systems, this geochemical behavior is quite favorable.

In the abiotic precipitate, a mixture of vaterite and calcite was obtained, and a single low-symmetry, incorporated species was identified by TRLFS. However, because this species has not been identified in previous studies or in the biogenic samples produced here, it cannot be definitively stated in which phase this species is incorporated. It is well-known that growth medium and synthetic conditions can have a significant impact on mineral phase, morphology, stability, etc.[52] during $CaCO_3$ precipitation, whereas the effect they might have on speciation of co-contaminants present during mineral formation has been considerably less studied. Although, recent investigations have shown that nitrate present even in trace amounts ($\sim 10^{-7}$ M) in the medium can effectively alter Eu^{3+} interactions and speciation with $CaCO_3$.[39] Future research should be aimed at also better understanding these phenomena.

The results presented here demonstrate that biomineralized $CaCO_3$ arising from MICP is capable of sequestrating Eu^{3+}, and hence this system should also behave similarly for other trivalent lanthanides and trivalent actinides. These findings reiterate that the interactions of these elements with minerals can be affected by the provenance and the conditions under which the mineral is formed. Thus, the unique interaction of biomineralized $CaCO_3$ with Eu^{3+} solidifies the need to further explore the role of biologically formed minerals in the near and far field of nuclear repository sites and how they interact with (radio)contaminants. It also demonstrates the importance of molecular level studies of diverse systems to be able to reliably describe (and predict) the behavior of biogeochemical systems.

454 ASSOCIATED CONTENT

455 **Supporting Information**. Light microscope images of precipitates and graphs of TGA, EDX,
456 TRLFS lifetime measurements of biogenic $CaCO_3$ with Eu^{3+} samples, and TRLFS excitation
457 spectrum of calcite produced without bacteria are provided. This material is available free of
458 charge via the Internet at http://pubs.acs.org.

459 AUTHOR INFORMATION

460 **Corresponding Author**

461 E-mail: moritz.schmidt@hzdr.de (MS), Phone: +49-351-260 3136

462 **Notes**

463 The authors declare no competing financial interest.

464 ACKNOWLEDGMENT

465 The authors would like to thank the Helmholtz-Zentrum Dresden-Rossendorf for the financial
466 support of EVJ. We gratefully acknowledge the Helmholtz Gemeinschaft Deutscher
467 Forschungszentren for supporting the Helmholtz-Nachwuchsgruppe “Structures and Reactivity at
468 the Water/Mineral Interface” (VH-NG-942). Special acknowledgement and thanks for those who
469 have contributed to the technical work and measurements supporting this paper: Stephan Weiss,
470 Karsten Heim, Andrea Scholz, Dr. Rene Hübner, Carola Eckardt, and Sabrina Gurlit.

471 REFERENCES

472 1. Lowenstam, H. A.; Weiner, S. In *On Biomineralization*. NewYork, NY: Oxford University
473 Press, **1989**.

2. Decho, A. W. Overview of biopolymer-induced mineralization: what goes on in biofilms? *Ecol. Eng*. **2010**, *36*: 137-144.

3. Benzerara, K.; Miot, J.; Morin, G.; Ona-Nguema, G.; Skouri-Panet, F.; Ferard, C. Significance, mechanisms and environmental implications of microbial biomineralization. *CR: Geosci*. **2011**, *343*, 160-7.

4. Dhami, N. K.; Reddy, M. S.; Mukherjee, A. Biomineralization of calcium carbonates and their engineered applications: a review. *Frontiers in microbiology* **2013,** *4*, 314.

5. Sarayu, K.; Iyer, N. R.; Murthy, A. R. Exploration on the biotechnological aspect of the ureolytic bacteria for the production of the cementitious materials--a review. *Appl. Biochem. Biotech.* **2014,** *172* (5), 2308-23.

6. Stocks-Fischer, S.; Galinat, J. K.; Bang, S. S. Microbiological precipitation of $CaCO_3$. *Soil Biol. Biochem*. **1999**, *31*, 1563–1571.

7. Fujita, Y.; Ferris, F. G.; Lawson, R. D.; Colwell, F. S.; Smith, R. W. Calcium carbonate precipitation by ureolytic subsurface bacteria. *Geomicrobiol. J.* **2000,** *17* (4), 305-318.

8. Mitchell, A. C.; Ferris, F. G. The influence of Bacillus pasteurii on the nucleation and growth of calcium carbonate. *Geomicrobiol. J.* **2006,** *23* (3-4), 213-226.

9. Lauchnor, E. G.; Schultz, L. N.; Bugni, S.; Mitchell, A. C.; Cunningham, A. B.; Gerlach, R. Bacterially induced calcium carbonate precipitation and strontium coprecipitation in a porous media flow system. *Environ. Sci. Technol.* **2013,** *47* (3), 1557-64.

10. Achal, V.; Pan, X. Influence of calcium sources on microbially induced calcium carbonate precipitation by Bacillus sp. CR2. *Appl. Biochem. Biotech.* **2014,** *173* (1), 307-17.

11. Burne, R. A.; Chen, Y. M. Bacterial ureases in infectious diseases. *Microbes and Infection*. **2000**, *2,* 533-42.

12. Parks, S. L. Kinetics of Calcite Precipitation by Ureolytic Bacteria under Aerobic and Anaerobic Conditions. MS Thesis. **2009**, Montana State University, Bozeman MT.

13. Warren, L. A.; Maurice, P. A.; Parmar, N.; Ferris, F. G. Microbially mediated calcium carbonate precipitation: implications for interpreting calcite precipitation and for solid-phase capture of inorganic contaminants. *Geomicrobiol. J.* **2001,** *18* (1), 93-115.

14. Rodriguez-Navarro, C.; Jimenez-Lopez, C.; Rodriguez-Navarro, A.; Gonzalez-Muñoz, M. T.; Rodriguez-Gallego, M. Bacterially mediated mineralization of vaterite. *Geochim. Cosmochim. Ac*. **2007,** *71* (5), 1197-1213.

15. Phillips, A. J.; Gerlach, R.; Lauchnor, E.; Mitchell, A. C.; Cunningham, A. B.; Spangler, L. Engineered applications of ureolytic biomineralization: a review. *Biofouling*. **2013**, *29* (6), 715-33.

16. Martin, D.; Dodds, K.; Butler, I. B.; Ngwenya, B. T. Carbonate precipitation under pressure for bioengineering in the anaerobic subsurface via denitrification. *Environ. Sci. Technol*. **2013,** *47* (15), 8692-9.

17. Kang, C. H.; Han, S. H.; Shin, Y.; Oh, S. J.; So, J. S. Bioremediation of Cd by microbially induced calcite precipitation. *Appl. Biochem. Biotech.* **2014,** *172* (6), 2907-15.

513 18. Kang, C. H., Oh, S. J., Shin, Y., Han, S., Nam, I. (2015). "Bioremediation of lead by
514 ureolytic bacteria isolated from soil at abandoned metal mines in South Korea."Ecol. Eng.
515 **2015**, *74*, 402-407.

516 19. Fujita, Y.; Redden, G. D.; Ingram, J. C.; Cortez, M. M.; Ferris, F. G.; Smith, R. W. Strontium
517 incorporation into calcite generated by bacterial ureolysis. *Geochim. Cosmochim. Ac*. **2004,**
518 *68* (15), 3261-70.

519 20. Fujita, Y.; Taylor, J.; Wendt, L.; Reed, D.; Smith, R. Evaluating the potential of native
520 ureolytic microbes to remediate Sr contaminated environment. *Environ. Sci. Technol*. **2010**,
521 *44*, 7652–8.

522 21. Mitchell, A. C.; Ferris, F. G. The coprecipitation of Sr into calcite precipitates induced by
523 bacterial ureolysis in artificial groundwater: Temperature and kinetic dependence. *Geochim.*
524 *Cosmochim. Ac*. **2005,** *69* (17), 4199-4210.

525 22. Aarkog, A.; Lippert, J. Europium-155 in debris from nuclear weapons. *Science*. **1967**,
526 *157(3787)*, 425-427.

527 23. Geckeis, H.; Lutzenkirchen, J.; Polly, R.; Rabung, T.; Schmidt, M. Mineral-water interface
528 reactions of actinides. *Chem. Rev.* **2013,** *113* (2), 1016-62.

529 24. Thein, M.; Beck, J. N.; Johnson, H.; Cooper, W. W.; Reynolds, M. A.; Clark, R. S.; Baugh, J.
530 O.; Kuroda, P. K. Fractionation of [atomic] bomb-produced rare-earth nuclides in the
531 atmosphere. *Environ. Sci. Technol*. **1969**, *3*, 667−670.

532 25. Thakur, P.; Lemons, B. G.; Ballard, S.; Hardy, R. Environmental and health impacts of
533 February 14, 2014 radiation release from the nation's only deep geologic nuclear waste
534 disposal. *J. Environ. Radioact.* **2015**, *146*, 6-15.

535 26. Bunzli, J. C. G.; Piguet, C. Taking advantage of luminescent lanthanide ions. *Chem. Soc.*
536 *Rev.* **2005**, *34*, 1048-1077.

537 27. Martin, R. B.; Richardson, F. S. Lanthanides as probes for calcium in biological systems. *Q.*
538 *Rev. Biophys.* **1979**, I2, 181-209.

539 28. Stumpf, T.; Marques Fernandes, M.; Walther, C.; Dardenne, K.; Fanghanel, T. Structural
540 characterization of Am incorporated into calcite: a TRLFS and EXAFS study. *J Colloid*
541 *Interf. Sci* **2006,** *302* (1), 240-5.

542 29. Stumpf, T.; Fanghanel, T. A time-resolved laser fluorescence spectroscopy (TRLFS) study of
543 the interaction of trivalent actinides (Cm(III)) with calcite. *J Colloid Interf. Sci* **2002,** *249* (1),
544 119-22.

545 30. Lakhstanov, L. Z.; Stipp, S. L. S. Experimental study of europium (III) coprecipitation with
546 calcite. *Geochim. Cosmochim. Ac.* **2004**, *68*, 819-827.

547 31. Elzinga, E. J.; Reeder, R. J.; Withers, S. H.; Peale, R. E.; Mason, R. A.; Beck, K. M.; Hess,
548 W. P. (2002) EXAFS study of rare-earth element coordination in calcite. *Geochim.*
549 *Cosmochim. Ac.* **2002**, *66*, 2875–2885.

32. Schmidt, M.; Stumpf, T.; Walther, C.; Geckeis, H.; Fanghanel, T. Phase transformation in $CaCO_3$ polymorphs: a spectroscopic, microscopic, and diffraction study. *J Colloid Interf. Sci* **2010,** *351* (1), 50-56.

33. Schmidt, M.; Stumpf, T.; Marques Fernandes, M.; Walther, C.; Fanghanel, T. Charge compensation in solid solutions. *Angew. Chem.* **2008,** *47* (31), 5846-50.

34. Piriou, B.; Fedoroff, M.; Jeanjean, J.; Bercis, L. Characterization of the sorption of europium(III) on calcite by site-selective and time-resolved luminescence spectroscopy. *J. Colloid Interf. Sci*. **1997**, *194* (2), 440–447.

35. Stipp, S. L. S.; Christensen, J. T.; Lakhstanov, L. Z.; Baker, J. A.; Waight, T. E. Rare Earth element (REE) incorporation in natural calcite: Upper limits for actinide uptake in a secondary phase. *Radiochim. Acta.* **2006**, *94*, 523-528.

36. Holliday, K.; Handley-Sidhu, S.; Dardenne, K.; Renshaw, J.; Macaskie, L.; Walther, C.; Stumpf, T. A new incorporation mechanism for trivalent actinides into bioapatite: a TRLFS and EXAFS study. *Langmuir.* **2012,** *28* (8), 3845-51.

37. Holliday, K. S.; Dardenne, K.; Walther, C.; Stumpf, T. The incorporation of europium into apatite: anew explanation. *Radiochim. Acta.* **2013,** *101* (4), 267-272.

38. Schmidt, M.; Stumpf, T.; Walther, C.; Geckeis, H.; Fanghanel, T. Incorporation versus adsorption: substitution of Ca^{2+} by Eu^{3+} and Cm^{3+} in aragonite and gypsum. *Dalton T.* **2009,** *33*, 6645-50.

569 39. Hofmann, S.; Voïtchovsky, K.; Schmidt, M.; Stumpf, T. Trace concentration – Huge impact:
570 Nitrate in the calcite/Eu(III) system. *Geochim. Cosmochim. Ac.* **2014,** *125*, 528-538.

571 40. Binnemans, K. Interpretation of europium(III) spectra. *Coord. Chem. Rev*. **2015**, *295*. 1-45.

572 41. Horrocks, W. D.; Sudnick, D. R. Lanthanide ion probes of structure in biology – laser-
573 induced luminescence decay constants provide a direct measure of the number of metal
574 coordinated water-molecules. *J. Am. Chem. Soc*. **1979**, *101*, 334–340.

575 42. Choppin, G. R.; Jensen, M. P. In *Chemistry of the Actinides and Transactinides*; Morss, L.
576 R., Edelstein, N. M., Fuger, J., Eds.; Springer: Dordrecht, Germany, **2006**; p 2528.

577 43. Ronholm, J.; Schumann, D.; Sapers, H. M.; Izawa, M.; Applin, D.; Berg, B.; Mann, P.; Vali,
578 H.; Flemming, R. L.; Cloutis, E. A.; Whyte, L. G. A mineralogical characterization of
579 biogenic calcium carbonates precipitated by heterotrophic bacteria isolated from cryophilic
580 polar regions. *Geobiology.* **2014,** *12* (6), 542-56.

581 44. Dickinson, S. R.; McGrath, K. M. Quantitative determination of binary and tertiary calcium
582 carbonate mixtures using powder X-ray diffraction. *The Analyst* **2001,** *126* (7), 1118-1121.

583 45. Huaxiao, Y.;Han, Z.; Zhao, H.; Zhou, S.; Chi, N.; Han, M.; Kou, X.; Zhang, Y.; Xu, L.;
584 Tian, C.; Qin, S. Characterization of calcium deposition induced by Synechocystis sp.
585 PCC6803 in BG11 culture medium. *Chinese Jour. Ocean. Limn*. **2014**, *32* (3): 503-510.

586 46. Stalport, F.; Coll, P.; Cabane, M.; Person, A.; González, R. N.; Raulin, F.; Vaulay, M. J.;
587 Ausset, P.; McKay, C. P.; Szopa, C.; Zarnecki, J. Search for past life on Mars: Physical and

588 chemical characterization of minerals of biotic and abiotic origin: part 1 - Calcite. *Geophys.*
589 *Res. Lett.* **2005,** *32* (23), L23305.

590 47. Astilleros, J. M., C. M. Pina, L. Fernandez-Diaz, and A. Putnis. Metastable phenomena on
591 calcite {1014} surfaces growing from Sr^{2+}-Ca^{2+}-CO_3^{2-} aqueous solutions, *Chem. Geol.*, **2002**,
592 *193*, 93–107.

593 48. Hofmann, S., Voïtchovsky, K., Spijker, P., Schmidt, M., Stumpf, T. Visualising the
594 molecular alteration of the calcite (104) – water interface by sodium nitrate. *Sci. Rep.* **2016**,
595 *6*, 21576.

596 49. Fernandes, M. M.; Schmidt, M.; Stumpf, T.; Walther, C.; Bosbach, D.; Klenze, R.;
597 Fanghanel, T. Site-selective time-resolved laser fluorescence spectroscopy of Eu^{3+} in calcite.
598 *J Colloid Interf. Sci* **2008,** *321* (2), 323-31.

599 50. Gilbert, P. U. P. A.; Abrecht, M.; Frazer, B. H. The Organic-Mineral Interface in
600 Biominerals. *Rev. Mineral. Geochem*. **2005**, *59*, 157-185.

601 51. Mann, S. In *Biomineralization: Principles and Concepts in Bioinorganic Materials*
602 *Chemistry*. Oxford Univ. Press, Oxford, **2001**.

603 52. Naka, K.; Chujo, Y. Control of crystal nucleation and growth of calcium carbonate by
604 synthetic substrates. *Chem. Mater.* **2001**, *13*, 3245-3259.

605

606 TOC

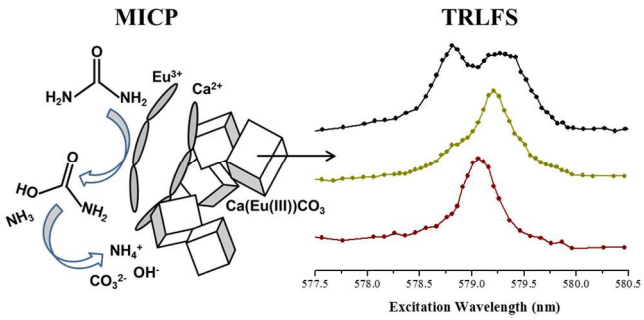
MICP
TRLFS
Eu3+
Ca2+
Ca(Eu(III))CO3
NH4+
CO32-
OH-
577.5
578.0
578.5
579.0
579.5
580.0
580.5
Excitation Wavelength (nm)

607

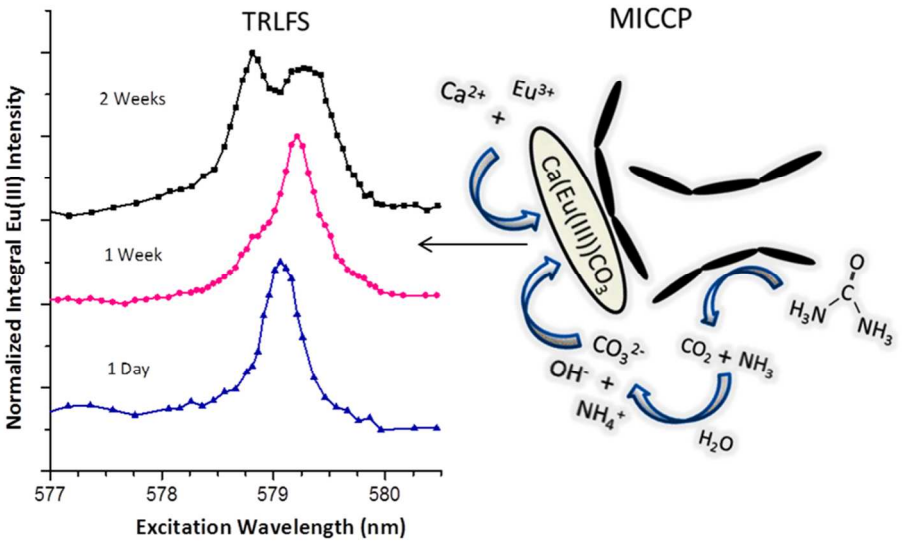

TOC graphic

227x131mm (150 x 150 DPI)